

Receptor-Based Modeling and 3D-QSAR for a Quantitative Production of the Butyrylcholinesterase Inhibitors Based on Genetic Algorithm

Zaheer-ul-Haq,^{*,†,§} Reaz Uddin,^{‡,§} Hongbin Yuan,^{||} Pavel A. Petukhov,^{||}
M. Iqbal Choudhary,[§] and Jeffry D. Madura[⊥]

Dr. Panjwani Center for Molecular Medicine and Drug Research, International Center for Chemical & Biological Sciences, University of Karachi, Karachi 75270, Pakistan, Department of Medicinal Chemistry and Pharmacognosy, College of Pharmacy, University of Illinois at Chicago, Chicago, Illinois 60612, and Department of Chemistry and Biochemistry, Center for Computational Sciences, Duquesne University, 600 Forbes Avenue, Pittsburgh, Pennsylvania 15282

Received January 7, 2008

Three-dimensional quantitative structure–activity relationship (3D-QSAR) models have been constructed using the comparative molecular field analysis (CoMFA) and comparative molecular similarity indices analysis (CoMSIA) for a series of structurally related steroidal alkaloids as butyrylcholinesterase (BuChE) inhibitors. Docking studies were employed to position the inhibitors into the BuChE active site to determine the most probable binding mode. The strategy was to explore multiple inhibitor conformations in producing a more reliable 3D-QSAR model. These multiple conformations were derived using the FlexS program. The conformation selection step for CoMFA was done by genetic algorithm. The genetic algorithm based CoMFA approach was found to be the best. Both CoMFA and CoMSIA yielded significant cross-validated q^2 values of 0.701 and 0.627 and the r^2 values of 0.979 and 0.982, respectively. These statistically significant models were validated by a test set of five compounds. Comparison of CoMFA and CoMSIA contour maps helped to identify structural requirements for the inhibitors and serves as a basis for the design of the next generation of the inhibitor analogues. The results demonstrate that the combination of ligand-based and receptor-based modeling with use of a genetic algorithm is a powerful approach to build 3D-QSAR models. These data can be used for the lead optimization process with respect to inhibition enhancement which is important for the drug discovery and development for Alzheimer's disease.

INTRODUCTION

Alzheimer's disease (AD) is a slowly progressive neurodegenerative disorder of the elderly. It is characterized by widespread loss of central cholinergic neuronal function.¹ The only symptomatic treatment proven to be effective to date is the use of cholinesterase inhibitors (ChEI) to augment surviving cholinergic activity.^{2,3} Two types of ChE enzyme are found in the Central Nervous System (CNS), acetylcholinesterase (AChE; EC 3.1.1.7) and butyrylcholinesterase (BuChE; EC 3.1.1.8).

AChE and BuChE share 65% amino acid sequence homology despite being encoded by different genes on human chromosomes 7(7q22) and 3(3q26), respectively.⁴ Acetylcholinesterase is responsible for the hydrolysis of acetylcholine at the synaptic cleft and the neuromuscular junction in response to nerve action potential,⁵ while the BuChE preferentially not only acts on butyrylcholine but also

hydrolyzes acetylcholine.⁶ In addition, both AChE and BuChE seem to be involved in roles that are independent of their catalytic activities, such as cell differentiation and development.^{7,8} BuChE and AChE are able to catalyze the hydrolysis of acetylcholine (ACh) at a rate of >10,000 molecules per second.⁹

Because BuChE is relatively abundant in plasma (about 3 mg/L) and can degrade a large number of ester-containing compounds, it plays important pharmacological and toxicological roles.¹⁰ For instance, BuChE is a potential detoxifying enzyme to be used as a prophylactic scavenger against neurotoxic organophosphates such as the nerve gas soman.^{10–12}

Previously, the relative contribution of BuChE to the regulation of ACh levels was largely ignored presumably due to unclear physiological function of BuChE.^{11–14} However, there is growing evidence that both enzymes regulate ACh levels and may also play a part in the development and progression of AD.¹⁵

In the normal brain, AChE represents approximately 80% of ChE activity with BuChE comprising the remainder.¹⁶ In advanced AD, however, AChE activity may be reduced to 55–67% of normal levels in specific brain regions, while BuChE activity increases.^{14–16} Cytochemical studies have revealed that in certain neuronal pathways of some species, BuChE replaces AChE.¹⁷ The BuChE may also have a role in the aggregation of β -amyloid protein (A β) that occurs in the early stages of senile plaque formation in AD.¹⁸ When

* Corresponding author fax: +92 21 4819018-19; e-mail: zaheer_qasmi@hotmail.com.

[†] Present address: Department of Chemistry and Biochemistry, Center for Computational Sciences, Duquesne University, 600 Forbes Ave., Pittsburgh, PA 15282.

[§] University of Karachi.

[‡] Present address: Department of Medicinal Chemistry and Pharmacognosy, College of Pharmacy, University of Illinois at Chicago, Chicago, IL 60612.

^{||} University of Illinois at Chicago.

[⊥] Duquesne University.

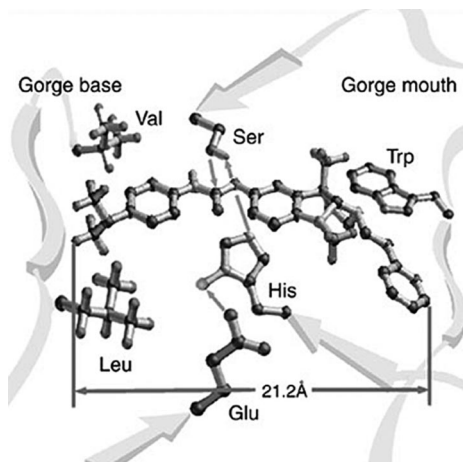


Figure 1. The gorge of BuChE and alignment of the BuChE specific inhibitor, phenethylcymserine, with the key amino acids to cause enzyme inhibition. The picture has been taken by the permission of N. H. Greig, principal author of the article referenced as 15.

BuChE is added to A β in tissue culture it amplifies A β neurotoxicity, pointing to a potentially valuable therapeutic role for BuChE inhibition in AD.¹⁹ Gene studies have identified a potential link between one of BuChEs (variant K) and susceptibility for developing AD.²⁰ The value of inhibiting BuChE has been demonstrated recently using experimental agents with enhanced selectivity for BuChE versus AChE (cymserine: 15-fold; bisnorcymserine: 110-fold; phenethylcymserine: 5000-fold)^{21,22} and BuChE-selective carbamates such as MF-8622.^{23,24} Selective inhibition of BuChE versus AChE derives from an ability to utilize the additional space present in the gorge of BuChE (Figure 1). These newly developed selective BuChE inhibitors have been evaluated in animal studies with promising results.^{24–27} Furthermore, as AD progresses, the increasing role that BuChE is considered to play in regulating brain ACh levels makes it a valuable target to ameliorate the cholinergic deficit and provide symptomatic benefits over the course of disease severity.¹⁵

From the resolved 3D structures of various cholinesterases, it is known that the active sites residues of these enzymes lay at the bottom of a 20 Å deep hydrophobic gorge.^{28–35} Due to a large cavity of this gorge BuChEs accept in comparison to AChEs a broader variety of substrates and inhibitors.^{36–38} For instance they metabolize butyrylcholine, the choline ester with a large acyl moiety whose hydrolysis by vertebrate AChEs is negligible.

Although a similar peripheral site has been described for human BuChE, site-directed mutagenesis and photoaffinity labeling studies showed that its location and the response upon ligand binding differ significantly from those of AChE.^{17,39}

Structure–activity analysis is the foundation for understanding the structural features of both the inhibitors and the target receptors involved in a particular biological process and thus helps to design more effective inhibitors.⁴⁰ It appears relatively difficult to find a reliable predictive model based on the calculated energies obtained by docking.^{41,42} To overcome this problem, highly predictive QSAR i.e., CoMFA⁴³ and CoMSIA⁴⁴ modeling techniques have been developed by using the technique of structure-based alignments of the substrates. These models can be used to identify

important protein–ligand interactions and are found to be consistent with the crystal structure of the protein–ligand complex.⁴⁵ The availability of X-ray crystal coordinates of inhibitors bound with the receptor have contributed to formulate effective predictive 3D-QSAR models based on (1) identification of possible conformations of related inhibitors in the active site and (2) understanding of the interactions of the inhibitors with the receptor in three-dimension.⁴⁶ A 3D-QSAR experiment performs two functions: the derivation of a statistically significant and highly predictive model that is used to estimate and rank new compounds for planned synthesis and the provision of an easily interpretable graphical tool which can identify a particular physicochemical property for increased affinity and selectivity.⁴⁷ These physicochemical properties include steric bulk, partial charge, local hydrophobicity, or hydrogen bond donor and acceptor.⁴⁸

The level-dependent contouring of usual CoMFA-field contributions highlights those regions in space where the aligned molecules would favorably or unfavorably interact with a possible environment. The CoMSIA field contributions identify those areas within the region occupied by the ligand that “favor” or “dislike” the presence of a group with a particular physicochemical property. This association of required properties with a possible ligand shape is a more direct indicator to check whether all features important for a particular activity are present in the structures under consideration.⁴⁴

The discovery of natural cholinesterase inhibitors has been a very challenging area of drug development due to the involvement of cholinesterases in Alzheimer’s disease and other related dementias. We have previously reported a number of new natural inhibitors of cholinesterases (AChE and BuChE) isolated from indigenous medicinal plants.^{49–53} The steady state inhibition kinetics, pharmacological profiles, SAR, 3D-QSAR, and molecular docking studies have been conducted on a similar series of compounds for AChE inhibition.^{54–57}

In the present study, two 3D-QSAR methods, CoMFA and CoMSIA, were applied and evaluated in order to accurately predict the inhibitory activity. For this reason a set of structurally similar butyrylcholinesterase inhibitors were used to create a predictive model. The results from this study will be helpful in the future for the design of new and more potent butyrylcholinesterase inhibitors. To the best of our knowledge this is the first attempt toward the establishment of 3D-QSAR for the butyrylcholinesterase inhibitors which may be used for the treatment of Alzheimer’s disease.

Docking is one method in which the binding of an inhibitor to a receptor can be explored.^{58–66} In CoMFA or other 3D-QSAR studies, the molecule alignment and conformation determination are so important that they affect the success of a model. In the present case, a bound complex of steroidal alkaloid/BuChE was not available, and therefore a computational method has to be implemented to determine possible conformations and alignment of a set of molecules so that 3D-QSAR can be carried out. Several strategies have been used in the past, to determine the conformation and alignment of molecules. Of them, docking is an attractive way to align molecules for CoMFA and/or CoMSIA. Several applications of docking alignment with CoMFA have been reported.^{67–71}

Recently, we used FlexX to successfully dock a set of steroidal alkaloid inhibitors into the active site gorge of

Table 1. BuChE Inhibitory Activities of Compounds 1–39

s. no.	compd no.	compd name	IC ₅₀ (μM)	pIC ₅₀	ref
Training Set					
1	SAR01	isosarcodine	1.89 ± 0.06	5.72	57
2	SAR02	iso- <i>N</i> -formylchoneformine	4.07 ± 0.11	5.39	49
3	SAR03	saracodine	12.51 ± 0.06	4.90	49
4	SAR04	sarcorine	10.33 ± 0.02	4.99	52
5	SAR05	<i>N</i> _a -demethylsaracodine	16.55 ± 0.20	4.78	52
6	SAR06	saracocine	3.86 ± 0.01	5.41	49
7	SAR07	saracodine	18.31 ± 0.74	4.74	57
8	SAR08	saligenamide-A	4.63 ± 0.07	5.33	52
9	SAR09	vaganine-A	2.32 ± 0.06	5.63	52
10	SAR10	saligcinamide	4.84 ± 0.12	5.32	52
11	SAR11	saligenamide-C	38.36 ± 0.74	4.42	52
12	SAR12	5,6-dehydrosarconidine	1.89 ± 0.06	5.72	49
13	SAR13	saligenamine	25.7 ± 0.63	4.59	49
14	SAR14	saligenamide-D	23.78 ± 0.15	4.62	52
15	SAR15	saligenamide-E	3.65 ± 0.02	5.44	52
16	SAR16	saligenamide-F	4.07 ± 0.11	5.39	52
17	SAR17	2β-hydroxyepipachysamine-D	28.96 ± 0.01	4.54	52
18	SAR18	salonine-B	4.50 ± 0.07	5.35	49,78
19	SAR19	salonine-A	32.70 ± 1.20	4.49	78
20	SAR20	salonine-C	32.20 ± 0.50	4.49	49
21	SAR21	salignarine-F	1.90 ± 0.20	5.72	49
22	SAR22	16-dehydrosarcorine	3.95 ± 0.53	5.40	50
23	SAR23	axillarine-C	17.99 ± 0.22	4.74	52
24	SAR24	axillarine-F	18.24 ± 0.01	4.74	52
25	SAR25	dictyophlebine	3.65 ± 0.02	5.44	49
26	SAR26	sarsalignone	4.29 ± 0.03	5.37	52
27	SAR27	nepapakistamine	25.00 ± 0.79	4.60	53
28	SAR28	sarcoveganin-C	1.50 ± 0.02	5.82	50
29	SAR29	salignarine-C	1.25 ± 0.01	5.90	51
30	SAR30	sarsalignone	2.18 ± 0.04	5.66	52
31	SAR31	<i>N</i> -methylformamidesalonine-B	10.50 ± 0.30	4.98	49
32	SAR32	5,14-dehydro- <i>N</i> _a -demethylsaracodine	25.00 ± 0.60	4.60	50
33	SAR33	axilliridine-A	2.49 ± 0.06	5.60	52
34	SAR34	14-dehydro- <i>N</i> _a -demethylsaracodine	10.10 ± 0.15	5.00	50
Test Set					
35	SAR35	vaganine-D	10.00 ± 0.120	5.00	53
36	SAR36	2-hydroxysalignarin E	6.91 ± 0.06	5.16	49
37	SAR37	epipachysamine-D	2.82 ± 0.02	5.55	49
38	SAR38	2-hydroxysalignamine	20.95 ± 3.20	4.68	51
39	SAR39	2,3-dehydrosarsalignone	32.20 ± 0.50	4.49	50

BuChE. A 3D-QSAR model was developed based on the docked conformation of the most active compound. In this paper we have performed CoMFA modeling utilizing the genetic algorithm (GA) in the selection of the ligand conformations. Previously this GA strategy has been utilized by Yuan et al.^{72,73} and found that this is very efficient in terms of the reliability of the CoMFA models. GA is inspired by natural selection in evolution.⁷⁴ GA approaches the optimum of a given function in the same way nature selects the individual fittest for the environment. The GA uses a blind search strategy, requiring no knowledge of the properties of the function to be optimized, thus enabling the algorithm to be applied to a variety of optimization problems from robot behavior to drug design.^{75–77}

MATERIALS AND METHODS

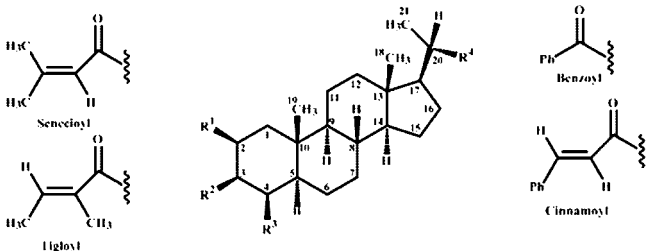
Biological Data. The BuChE inhibitory data, represented by IC₅₀ (μM), were obtained from recently published data^{49–53,57,78} (Table 1). The structures of potential inhibitors are presented in Table 2. The pIC₅₀ (−logIC₅₀) values were used to derive 3D-QSAR models. From a total of 39 compounds, a training set was created with 34 compounds, while 5 other compounds were used as the test set (Table

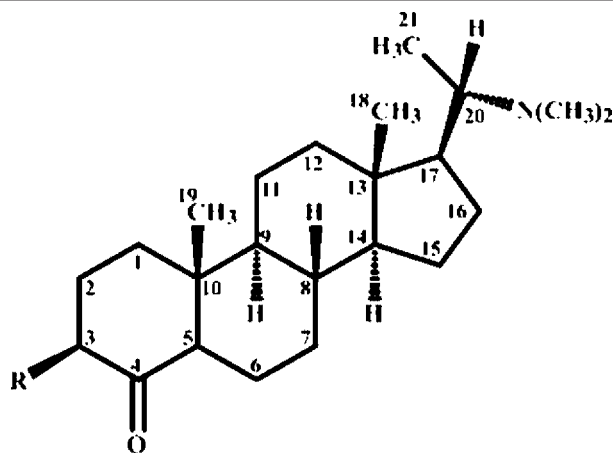
1). This test set was used to validate the predictive ability of the training set.

Modeling Tools. All molecular modeling and comparative molecular field evaluations were performed using SYBYL 7.2,⁷⁹ running on AMD Athlon (tm) workstation. The aliphatic amine groups of all compounds were considered protonated. Geometry optimizations were performed using the Tripos force field⁸⁰ with a distance-dependent dielectric and the Powell conjugate gradient algorithm. Gasteiger–Huckel charges were used. All water molecules, sulfate and chloride anions, glycerol, fucose, *N*-acetyl-*D*-glucosamine, and 2-(*N*-morpholino)ethanesulfonic acids were removed from the original protein data bank file.

Docking. FlexX, incremental construction algorithm,⁸¹ was used to get the appropriate binding conformations of the steroidal alkaloids inhibitors into the BuChE binding pocket. The crystal structure of human BuChE (PDB code: 1P0I) was used. One of the most active compounds, SAR29 (Figure 2a), was docked into the binding pocket, and the best conformation was used as a template to aligning rest of the compounds. The FlexX scoring function was used to select the best conformation. Prior to docking the inhibitors with the protein crystal structure, a redocking of the

Table 2. Chemical Structures of Compounds 1–39

						
compd no.	R ¹	R ²	R ³	R ⁴	unsaturation	ref
SAR01	H	NCH ₃ Ac	H	N(CH ₃) ₂		57
SAR02	H	N(CH ₃) ₂	H	NHCHO		49
SAR03	H	N(CH ₃) ₂	H	N(CH ₃) ₂	Δ ^{5,6}	49
SAR04	H	NHAc	H	N(CH ₃) ₂		52
SAR05	H	NHCH ₃	H	NCH ₃ Ac		52
SAR06	H	N(CH ₃) ₂	H	NCH ₃ Ac	Δ ^{5,6}	49
SAR07	H	N(CH ₃) ₂	H	NCH ₃ Ac		57
SAR08	H	NHCOCH=CCH ₃ CH(CH ₃) ₂	H	N(CH ₃) ₂		52
SAR09	H	HN-senecioid	OAc	N(CH ₃) ₂		52
SAR10	H	CH ₃ N-cinnamoyl	H	N(CH ₃) ₂		52
SAR11	OH	HN-tigloil	OAc	N(CH ₃) ₂	Δ ^{14,15}	52
SAR12	H	NHCH ₃	H	N(CH ₃) ₂	Δ ^{16,17}	49
SAR13	H	OCH ₃	H	NHCH ₃	Δ ^{5,6} & Δ ^{16,17}	49
SAR14	α-OH	HN-Tigloil	H	N(CH ₃) ₂	Δ ^{4,5} & Δ ^{16,17}	52
SAR15	H	N(CH ₃)COCH=C(CH ₃)CH(CH ₃) ₂	H	N(CH ₃) ₂	Δ ^{16,17}	52
SAR16	H	N(CH ₃)COCH=C(CH ₃)CH(CH ₃) ₂	H	N(CH ₃) ₂		52
SAR17	OH	HN-benzoyl	H	N(CH ₃) ₂		52
SAR18	H	OCH ₃	H	N(CH ₃) ₂	Δ ^{5,6} & Δ ^{16,17}	49,78
SAR19	OH	HN-tigloil	OH	N(CH ₃) ₂	Δ ^{14,15}	78
SAR20	H	HN-tigloil	H	N(CH ₃) ₂	Δ ^{4,5} & Δ ^{14,15}	49
SAR21	H	HN-tigloil	OH	N(CH ₃) ₂	Δ ^{5,6}	49
SAR22	H	NHCOCH ₃	H	N(CH ₃) ₂	Δ ^{16,17}	50
SAR23	OH	HN-benzoyl	OAc	N(CH ₃) ₂		52
SAR24	OH	HN-tigloil	OAc	N(CH ₃) ₂		52
SAR25	H	NHCH ₃	H	N(CH ₃) ₂		49
SAR27	OAc	HN-tigloil	OAc	NHCH ₃	Δ ^{16,17}	53
SAR29	OH	HN-senecioid	H	N(CH ₃) ₂	Δ ^{5,6}	51
SAR31	H	OCH ₃	H	NCH ₃ (CHO)	Δ ^{5,6} & Δ ^{16,17}	49
SAR32	H	NHCH ₃	H	NCH ₃ Ac	Δ ^{5,6} & Δ ^{14,15}	50
SAR34	H	NHCH ₃	H	NCH ₃ Ac	Δ ^{14,15}	50
SAR35	H	HN-senecioid	OAc	N(CH ₃) ₂	Δ ^{16,17}	53
SAR36	OH	HN-tigloil	H	N(CH ₃) ₂	Δ ^{4,5}	49
SAR37	H	HN-benzoyl	H	N(CH ₃) ₂		49
SAR38	OH	OCH ₃	H	N(CH ₃) ₂	Δ ^{5,6} & Δ ^{16,17}	51



compd no.	R	unsaturation	ref
SAR26	HN-tigloil	Δ ^{5,6} & Δ ^{14,15}	52
SAR28	HN-tigloil	Δ ^{2,3} & Δ ^{16,17}	50
SAR30	HN-tigloil	Δ ^{5,6}	52
SAR33	HN-benzoyl	Δ ^{2,3}	52
SAR39	HN-tigloil	Δ ^{2,3} & Δ ^{5,6}	50

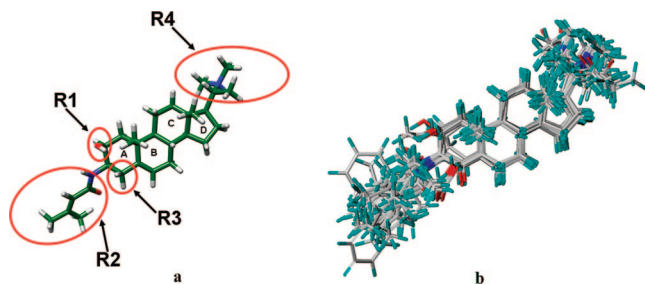


Figure 2. a) Salignarine-C (SAR29) was used as a template for alignment of all other structures. The important regions of the parent skeleton are also circled here as R1, R2, R3, and R4. b) Superposition of all BuChE inhibitors aligned by flexible superposition method by FlexS, in which all molecules are aligned onto the docked conformation of the most active compound.

cocrystallized ligand with 1POI was done to validate the docking protocol. The topmost docked solution was found in good agreement with the crystal structure of the cocrystallized ligand. The rmsd between the docking solution and the crystal structure was 1.53 Å.

Conformational Sampling and Alignment. The selected pose for SAR29 was used as a template in structure alignment for all molecules in the series. This step was performed by using an incremental construction algorithm and a scoring function based on intermolecular interactions and overlapping density functions implemented in the Flexible Superposition (FlexS) technique.⁸² The minimum volume overlap was set at 0.6, and the number of alignments per ligand was used initially as 30 (default) but was changed for the cases where optimum alignment was not obtained. The Gasteiger–Huckel charges were calculated during conformational alignment with FlexS. A top-ranked conformer for each compound was initially utilized for CoMFA modeling, and then the ten best conformations were used in order to explore all possible conformational space for each compound. The ten best poses were selected based on the following: (1) FlexS ranks and (2) if the pose is correctly oriented on the template. Figure 2b represents the alignment of the molecules.

CoMFA Modeling Based on Genetic Algorithm. The overall strategy for CoMFA modeling is shown as a scheme in the Supporting Information. A brief description of the procedure is outlined here. To explore the multiple conformations of the ligands, a genetic algorithm analysis was applied in the selection of the ligand conformations for the CoMFA. The genetic algorithm consisted of the following steps:

Initialization: This step generates an initial population P_i of CoMFA models using one randomly selected conformation among the ten conformations of each ligand. The population size was set to 100.

Iterations:

Crossover: Exchange the conformations of corresponding ligands for any two models in the population P_i . The crossover ratio was set to 50:50.

Mutation: For randomly selected ligands, replace the conformations obtained in step 1 with randomly selected conformations in the database. Store the results as a temporary population P_{tmp} . The mutation rate was set to 0.05.

Selection: Generate new CoMFA models for P_{tmp} . Compare their q^2 values with those generated for population P_i and keep the best models in population P_{i+1} .

Until: The 100 generations limit is reached or the best model remains unchanged for 10 consecutive generations.

CoMFA Fields. A training set of 34 compounds (Table 1) was selected from the existing database, representing the diversity of structures and activities. After alignment, the molecules were inserted as rows of a QSAR table along with their respective IC_{50} values (as pIC_{50}). CoMFA steric and electrostatic fields were calculated as described below and entered as columns in the QSAR table. Standard steric and electrostatic CoMFA field energies of each inhibitor were calculated using an sp^3 probe atom with a +1 charge at all intersections in regularly spaced (2.0 Å) grids surrounding each molecule. Lennard-Jones 6–12 potential and coulombic potential functions, within the Tripos force field⁸⁰ and a distance dependent ($1/r$) dielectric constant, were used in the calculation. The grid box dimensions were determined by the “create automatically” features in the CoMFA module within the “SYBYL” program. The same grid box was used in all calculations. An energy cutoff of 30 kcal/mol for both steric and electrostatic contributions was set as threshold, and the electrostatic terms were dropped within regions of steric maximum i.e., 30 kcal/mol. Five additional inhibitors (Table 1) were selected as a predictive set to test the robustness of the resulting model. They were aligned with the template (SAR29) structure using the same alignment protocol as described earlier, and finally their activities were predicted.

CoMSIA Fields. Another 3D-QSAR procedure, CoMSIA, can avoid some inherent deficiencies arising from the functional forms of Lennard-Jones and Coulomb potentials used in CoMFA. In CoMSIA, a distance dependent Gaussian-type functional form has been introduced. This can avoid singularities at the atomic positions and the dramatic changes of potential energy due to grids in the proximity of the surface. Meanwhile, no arbitrary definition of cutoff limits is required in CoMSIA, and the contour maps of the relative spatial contributions of the different fields can be substantially improved. This is essential for the interpretation in terms of separate property fields. The procedures of getting a 3D-QSAR model from a CoMSIA can be summarized into the following three steps.

First, all molecules are structure-based or field-based aligned.

Then, an evenly spaced rectangular grid is generated to enclose the molecular aggregate. A probe atom is placed at every lattice point to measure the electrostatic, steric, hydrophobic, and H-bond donor or acceptor fields.

Finally, the results from the field samplings are combined with the biological activities from the tested compounds and are put into a table, and partial least-squares (PLS) fitting is applied to obtain the final CoMSIA model.

To choose the appropriate components and to check the statistical significance of the models, leave-one-out cross-validations were used by PLS. Then, the final 3D-QSAR model was derived from the no cross-validation calculations. The CoMSIA results are finally interpreted graphically by field contribution maps using the field type “stdev*coeff”.

Similar to the usual CoMFA approach, a data table has been constructed from similarity indices⁴⁷ calculated via a common probe atom that is placed at the intersections of a regularly spaced lattice. A grid spacing of 2 Å has been used throughout this study. Similarity indices $A_{F,K}$ between the

compounds of interest and a probe atom, systematically placed at the intersections of the lattice, have been calculated according to eq 1 (e.g., at grid point q for molecule j of the data set)

$$A_{FK}^q(j) = -\sum_i \omega_{\text{probe},k} \omega_{ik} (e^{-\alpha r_{iq}})^2 \quad (1)$$

where i = the summation index over all atoms of the molecule j under investigation; ω_{ik} = the actual value of the physicochemical property k of atom i ; $\omega_{\text{probe},k}$ = the probe atom with charge +1, α = the attenuation factor; and r_{iq} = the mutual distance between probe atom at grid point q and atom i of the test molecule. Large values of α will result in a strong attenuation of the distance-dependent consideration of molecular similarity. Accordingly, there is little averaging of local feature matches of the molecules being compared. With small values of α also remote parts of each molecule will be experienced by the probe, and the global molecular features become more important. In the present study the α has been set at 0.3. With this selection, at a given lattice point the property value of an atom of the molecule under investigation (e.g., the partial atomic charge) is experienced in 1 Å distance by 74.1%, in 2 Å by 30.1% and in 3 Å by 6.7% of its total value. This permits a reasonable “local smearing” of the molecular similarity indices and should help to avoid extreme dependencies on small changes of the mutual alignments.⁴⁸ In the present study five physicochemical properties k (steric, electrostatic, hydrophobic and hydrogen bond donor and acceptor) were evaluated, using a common probe atom with 1 Å radius and charge, hydrophobicity and hydrogen-bond property of +1. Steric property fields were expressed by the third power of the atomic radii. Local hydrophobicities were associated using atom-based parameters developed by Viswanadhan et al.⁸³

Statistical Analysis/PLS. Correlations were derived using the method of Partial Least Squares (PLS)⁸⁴ and cross-validated to reduce the probability of obtaining chance correlations.

As used in this report, the cross-validated q^2 refers to the squared correlation coefficient of the equation derived from the cross-validation of the training set to determine the optimum number of principal components. The conventional r^2 is the fitted correlation of the training set using the optimum number of principal components with no cross-validation. The predictive r -squared was calculated by eq 2.

$$\text{predictive } r - \text{squared} = \text{ssd} - \text{press}/\text{ssd} \quad (2)$$

RESULTS AND DISCUSSION

Docking. The best docking solution showed that BuChE accommodates the studied compound inside the active site cavity. The best docking pose for SAR29 inside the binding pocket of BuChE is shown in Figure 3. The compound enters the cavity preferably by ring A. This might contribute highly to the stabilization of the complex since the steroid backbone of the ligand is highly hydrophobic due to its aliphatic character and therefore not well hydrated. The main hydrophobic interactions between the hydrocarbon skeleton of the inhibitors and the BuChE were observed with the most common residues Thr-120, Tyr-332, Trp-430, Ala-328, and Phe-329.

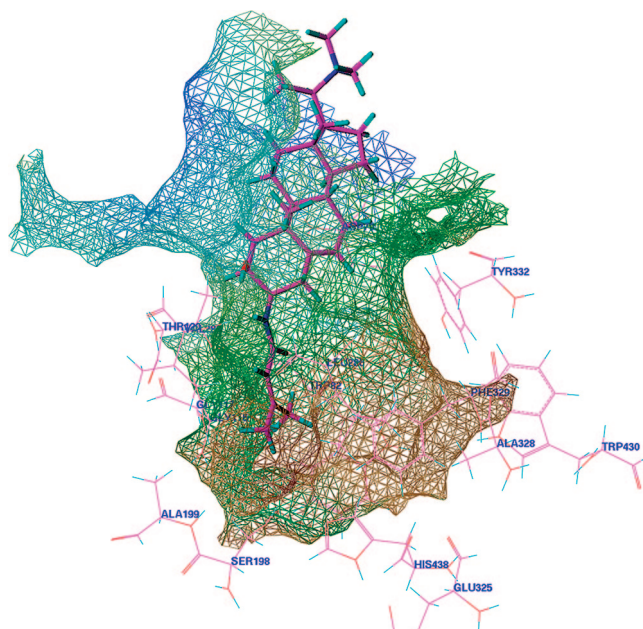


Figure 3. Docked pose of the most active compound (SAR29) inside the binding pocket of BuChE, generated by FlexX. Important interacting amino acid residues are displayed in magenta. The MOLCAD surface of the residues was generated by the fast molecular surface electron density method implemented in SYBYL7.2. The surface is mapped by its lipophilic potential. This docked conformation was further used as a template to overlay rest of the compounds by FlexS (PDB: 1POI).

Table 3. Summary of Statistics and Field Contributions for the Top Four CoMFA Models

parameters	Model9	Model21	Model72	Model80
q^2_a	0.902	0.911	0.730	0.701
r^2_b	0.998	0.998	0.994	0.979
SEE ^c	0.022	0.020	0.040	0.072
F -value ^d	2326.92	2957.134	738.562	264.356
no. of components ^e	6	6	6	5
<u>fraction^f</u>				
steric	0.499	0.484	0.500	0.531
electrostatic	0.501	0.516	0.500	0.469
predictive r -squared ^g	0.441	0.523	0.311	0.682
PRESS ^h	0.384	0.328	0.475	0.218

^a Cross-validated correlation coefficient. ^b Noncross-validated correlation coefficient. ^c Standard error of estimate. ^d F -test value.

^e Optimum number of components obtained from cross-validated PLS analysis and the same used in final noncross-validated analysis.

^f Field contributions. ^g Correlation coefficient for test set predictions.

^h Predicted residual sum of squares.

COMFA OF INHIBITORS

Model Selection. The CoMFA based on GA resulted in several models, and among them the final model selection is an important issue. Based on q^2 values, four different models have been selected for subsequent studies. Among them, models 72 and 80 were obtained with the cutoff $q^2 \geq 0.65$ and the other two models 9 and 21, with the cutoff $q^2 \geq 0.90$.

The external predictivity of the CoMFA model is extremely important in terms of the applicability of the CoMFA model. Therefore, it was decided to use the predictive- r^2 as a criterion for final selection of the one best model. As reflected by Table 3, model 80 has the highest predictive- r^2 value and hence the lowest PRESS value for the test set predictions. Therefore model 80 was selected as the best

Table 4. Results of the CoMFA and CoMSIA Analyses for the Compounds Used in the Training Set

parameters	CoMFA S, E ^h	CoMSIA				
		S, E, H, D, A ^h	S, E ^h	S, E, H ^h	S, E, H, A ^h	S, E, H, D ^h
q^2 ^a	0.701	0.627	0.382	0.444	0.386	0.615
SEP ^b	0.273	0.305	0.393	0.373	0.392	0.310
no. of components ^c	5	5	5	5	5	5
r^2 ^d	0.979	0.982	0.880	0.927	0.924	0.967
SEE ^e	0.072	0.085	0.174	0.135	0.138	0.090
field contributions	0.531, 0.469	0.064, 0.173, 0.135, 0.373, 0.255	0.330, 0.670	0.211, 0.393, 0.396	0.122, 0.237, 0.251, 0.390	0.102, 0.246, 0.197, 0.456
F -value ^f	264.356	185.867	40.877	70.649	68.035	166.192
predictive r -squared ^g	0.682	0.453	0.228	0.529	0.048	0.774

^a Cross-validated correlation coefficient. ^b Standard error of predictions. ^c Optimum number of components obtained from cross-validated PLS analysis and the same used in final noncross-validated analysis. ^d Noncross-validated correlation coefficient. ^e Standard error of estimate. ^f F -test value. ^g Correlation coefficient for test set predictions. ^h CoMFA and CoMSIA with different field contributions such as steric (S), electrostatic (E), hydrophobic (H), donor (D), and acceptor (A) fields.

CoMFA model. In addition to studying the effect of charges on 3D-QSAR studies, different methods were employed to calculate the charges on ligands included in this study. Quantitative comparisons of the charges calculated by different methods are reported in the Supporting Information. Different charges resulting from different calculation methods may influence the results of CoMFA as well as CoMSIA, but there are no significant effects of charges that were observed during our study for this particular steroidal class of compounds.

Predictive Power of the CoMFA Model. The final results of the CoMFA analysis with a 2.0 Å grid spacing are shown in Table 4. PLS analysis yielded consistent results. The optimal components that produce the best cross-validation linear regression coefficient were used to produce the noncross-validated model. The leave-one-out cross-validated PLS analysis results in a q^2 of 0.701 using five principal components, and the noncross-validated PLS analysis yields a higher r^2 of 0.979 with a standard error of estimate (SEE) 0.072. The inhibitory activity (pIC_{50}), the calculated activities using the CoMFA model, and the residual values for the training set and the test set are listed in Table 5. Graphic representation of observed vs calculated inhibitory activity is shown in Figure 4. The best selected 3D-QSAR model shows good prediction for the five tested compounds, which reflects that the derived model was satisfactory enough with respect to statistical significance and actual predictive ability.

Graphical Interpretation of the Results (CoMFA). The CoMFA steric and electrostatic fields from the final noncross-validated analysis were plotted as three-dimensional colored contour maps in Figure 5a. The field energies at each lattice point were calculated as the scalar results of the coefficient and the standard deviation associated with a particular column of the data table ($\text{stdev} \times \text{coeff}$), plotted as the percentage of contribution to the CoMFA equation. These maps show regions where differences in molecular fields are associated with differences in biological activity.

The steric interactions are represented by the colors green and yellow, while electrostatic interactions are represented by the colors red and blue (Figure 5a). In the green regions of steric contour plot, the bulky substituent enhances biological activity, while the bulky substituent in the yellow regions is likely to decrease activity. The green steric contour near the substituent at C20 of the D ring indicates that any bulky substituent is preferred at this position. This may

provide more possibilities to establish hydrophobic interactions with the peripheral site of the target protein. This observation is consistent with the experimental findings as compound SAR13 is less active than SAR38 because SAR13 is having a less bulky substituent at C20 than SAR38.

In an electrostatic contour map blue-colored contours represent regions where electropositive groups increase activity, whereas red-colored regions represent areas where electronegative groups enhance activity. The electrostatic contour plot on the set of compounds showed that there is a red-colored region situated close to the substituent at C3 that is to say, the negative charges at this region are in a high demand for ligand binding, and a charge withdrawing group linked to this position will enhance the biological activity. This observation also correlates with the experimental determinations, for example, the compound SAR37 is more active than compound SAR17. The only difference in both of them is the presence of a hydroxyl group at C-2 in compound SAR17 which makes SAR17 less active than SAR37 since the C-2 position is covered by the blue contour map. On the other hand, a negative group at the C-4 position makes compound SAR26, SAR28, SAR30, and SAR33 the most active compounds among the listed compounds. The presence of a double bond between C-5 and C-6 makes compound SAR06 more active than compound SAR07, which has an otherwise identical structure.

COMSIA OF INHIBITORS

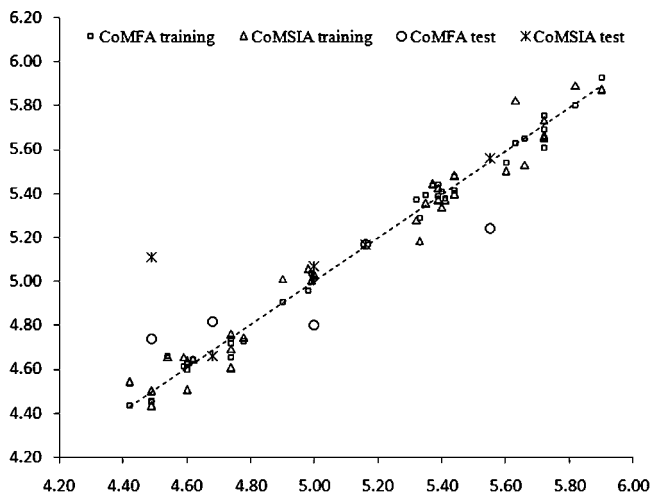
Predictive Power of the CoMSIA Model. The final results of the CoMSIA analysis with a 2.0 Å grid spacing are shown in Table 4. PLS analysis yielded consistent results. The optimal components that produce the best cross-validation linear regression coefficient were used to produce the noncross-validated model. The leave-one-out cross-validated PLS analysis results in a q^2 of 0.627 using five principal components, and the noncross-validated PLS analysis yields a higher r^2 of 0.982. The inhibitory activity (pIC_{50}), the calculated activities using the 3D-QSAR model from CoMSIA, and the residual values for the training and the test set are listed in Table 5. Correlation between observed vs calculated inhibitory activities are represented in a graphical manner in Figure 4. The best 3D-QSAR model has a good prediction for the five tested compounds. So the derived model was satisfactory with respect to statistical significance and actual predictive ability.

Table 5. Comparison of Experimental and Calculated Biological Activities of Compounds 1–39 by Using CoMFA and CoMSIA Analysis

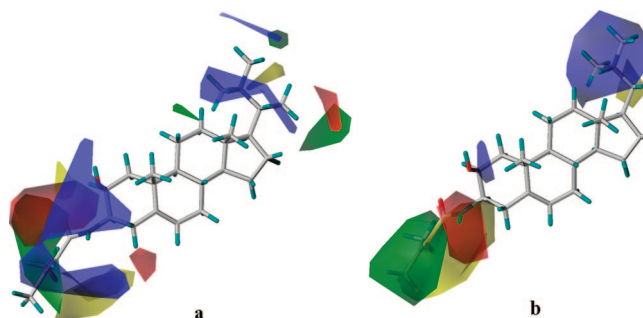
s. no.	compound	actual pIC ₅₀	CoMFA predicted pIC ₅₀	residual	CoMSIA predicted pIC ₅₀	residual
Training Set						
1	SAR01	5.72	5.61	0.11	5.65	0.07
2	SAR02	5.39	5.44	−0.05	5.43	−0.04
3	SAR03	4.90	4.90	0.00	5.01	−0.11
4	SAR04	4.99	5.04	−0.04	5.01	−0.01
5	SAR05	4.78	4.73	0.05	4.75	0.03
6	SAR06	5.41	5.38	0.03	5.37	0.04
7	SAR07	4.74	4.72	0.02	4.76	−0.02
8	SAR08	5.33	5.29	0.04	5.19	0.15
9	SAR09	5.63	5.63	0.00	5.82	−0.19
10	SAR10	5.32	5.37	−0.05	5.28	0.04
11	SAR11	4.42	4.44	−0.02	4.54	−0.12
12	SAR12	5.72	5.75	−0.03	5.67	0.05
13	SAR13	4.59	4.62	−0.03	4.66	−0.07
14	SAR14	4.62	4.65	−0.03	4.65	−0.03
15	SAR15	5.44	5.42	0.02	5.48	−0.04
16	SAR16	5.39	5.39	0.00	5.37	0.02
17	SAR17	4.54	4.66	−0.12	4.66	−0.12
18	SAR18	5.35	5.39	−0.04	5.36	−0.01
19	SAR19	4.49	4.45	0.04	4.43	0.06
20	SAR20	4.49	4.46	0.04	4.50	−0.01
21	SAR21	5.72	5.69	0.03	5.74	−0.02
22	SAR22	5.40	5.41	−0.01	5.34	0.06
23	SAR23	4.74	4.74	0.00	4.69	0.05
24	SAR24	4.74	4.65	0.09	4.61	0.13
25	SAR25	5.44	5.48	−0.04	5.40	0.04
26	SAR26	5.37	5.43	−0.06	5.45	−0.08
27	SAR27	4.60	4.62	−0.02	4.64	−0.04
28	SAR28	5.82	5.80	0.02	5.89	−0.07
29	SAR29	5.90	5.93	−0.03	5.87	0.03
30	SAR30	5.66	5.65	0.01	5.53	0.13
31	SAR31	4.98	4.96	0.02	5.06	−0.08
32	SAR32	4.60	4.60	0.00	4.51	0.09
33	SAR33	5.60	5.54	0.06	5.50	0.10
34	SAR34	5.00	5.01	−0.01	5.03	−0.03
Test Set						
35	SAR35	5.00	4.80	0.20	5.07	−0.07
36	SAR36	5.16	5.17	−0.01	5.17	−0.01
37	SAR37	5.55	5.24	0.31	5.56	−0.01
38	SAR38	4.68	4.82	−0.13	4.66	0.02
39	SAR39	4.49	4.74	−0.24	5.11	−0.62

Graphical Interpretation of the Results (CoMSIA). The CoMSIA steric and electrostatic fields based on PLS analyses are represented as 3D contour plots in Figure 5b.

In the electrostatic contour map, the positive charge can appear closer to the regions of positive coefficients (blue),

**Figure 4.** Plots of the predicted versus experimental activity data of 3D-QSAR from both CoMFA and CoMSIA for the training and the test compounds.

and the negative charge can be moved closer to the regions of negative coefficients (red). A close inspection of the electrostatic contour plots (Figure 5b) reveals that for the tested molecules the electropositive groups are more preferred, and the appearance of the blue regions near R4 zone

**Figure 5.** a) The CoMFA (stdev*coeff) steric and electrostatic contour plots. The favorable steric areas are shown in green, and the disfavored steric areas are shown in yellow. The positive potential favored areas are shown in blue, and the positive potential disfavored areas are shown in red. The most active compound in the series (SAR29) is shown as the reference compound. b) The CoMSIA (stdev*coeff) steric and electrostatic contour plots. The color scheme is the same as in Figure 5a. The most active compound in the series (SAR29) is shown as the reference compound.

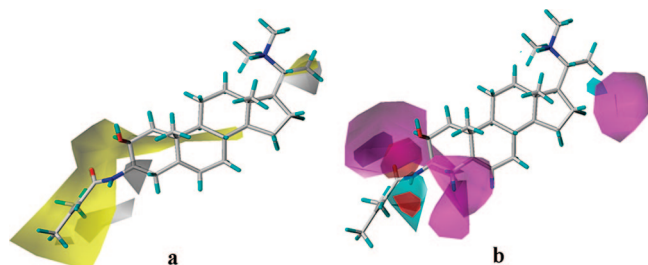


Figure 6. a) The CoMSIA (stdev*coeff) hydrophobic contour plots. The favorable hydrophobic areas are indicated by yellow color, whereas the disfavored hydrophobic areas are shown by white color. The most active compound (SAR29) is shown as the reference compound. b) The contour plots of the CoMSIA (stdev*coeff) H-bond donor and acceptor fields. The favorable H-bond donor is shown in cyan, and the unfavorable H-bond donor is shown in purple. The favorable H-bond acceptor is shown in magenta, and the unfavorable H-bond acceptor is in red. The most active compound (SAR29) is shown as the reference compound.

indicates that a more positive charge group substituted at these zones on the parent skeleton will enhance the biological activity.

In the steric contour map, it can be seen that the areas (green contour) correspond to regions where steric occupancy with bulky groups are preferred and that the areas encompassed by yellow contour should be sterically avoided. For the studied compounds on ring A, there exist two contour areas, a larger favorable area near the group substituted at the C3 on the ring A, and at the opposite site, a relatively smaller unfavorable area. Due to the steric complementarity between receptor and inhibitor, the positions which are encompassing the green region are sterically preferred to produce good steric interactions with the receptor and hence increase the inhibitory activity. By observing the steric contour map with the compound SAR29 (one of the most active compounds; Figure 2a), it can be readily seen that the green contour covered the whole carbonyl and the double bond region at the senecieryl group, while the terminal substituent on the double bond in the senecieryl group is covered by the yellow contour. The green area is indicating that the bulky substituent at the double bond but adjacent to the carbonyl position will enhance the biological activity. Similarly, a smaller terminal substituent on the double bond will enhance the inhibitory activity. For example, the structure of the compound SAR12 has a relatively small substituent, in the form of -NHCH_3 , at C3, while SAR35 has a bulky substituent in the form of the senecieryl group, which shows less inhibitory activity than compound SAR12. The same is observed if we compare the compound SAR25 with SAR35.

The contour map of hydrophobic properties indicates (Figure 6a) one distinct hydrophobically favorable site, a larger region near the R2 zone, which means that groups with high hydrophobicity (indicated by yellow contour in Figure 6a) will favor biological activity. It can be reasonably presumed that ring A combined with a substituent on it is composed of a large hydrophobic core and will produce a strong hydrophobic interaction with the receptor. This observation is also consistent with the CoMFA steric contour map (Figure 5a) in which the sterically more crowded substituent is necessary to enhance the biological activity at the same R2 zone.

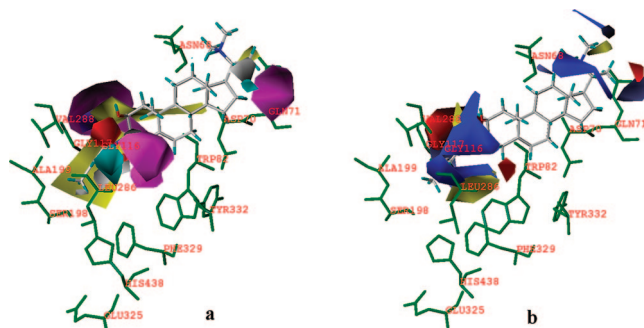


Figure 7. a) CoMSIA contour plots superimposed within the active site of BuChE with compound SAR29 and b) CoMFA contour plots superimposed within the active site of BuChE with compound SAR29.

The graphical interpretations of the field contributions of the H-bond properties are shown in Figure 6b as both H-bond donor and H-bond acceptor fields. In principle, they should highlight the areas beyond the ligands where putative hydrogen partners in the enzyme can form H-bonds that influence binding affinity. The hydrogen bond donor and acceptor fields showed the favorable (cyan) area near the amido group, and the H-bond acceptor field showed the favorable (magenta) area around the oxygen atom in amido group (Figure 6b). This may be due to the involvement of hydrogen bonding during interaction with target.

Superimposition of the CoMFA and CoMSIA coefficient contour maps on the ligand in the active site of BuChE (Figure 7 a,b) additionally supports the result that most of the interactions are hydrophobic in nature, and the residues nearby the hydrophobic favorable area mostly consist of hydrophobic amino acids (i.e., Gly, Val, and Leu). As depicted in Figure 7a,b, the substituents at position R2 are placed in the hydrophobic pocket formed by Leu286, Gly116, Gly117, Val288, and Ala199. A green color contour map of the CoMFA model (Figure 5a) and similarly of the green contour of CoMSIA (Figure 5b) appeared at this position suggesting bulky substituents at this position. Another yellow color CoMSIA contour near the same R2 region suggested the favorable hydrophobic interaction with the receptor hydrophobic pocket which is formed by the same amino acid residues. Most of the amino acid residues near the yellow contour regions are hydrophobic in nature e.g., Gly, Val, and Leu.

CONCLUSION

The present study correlates the BuChE inhibitory activities of the isolated natural compounds with the steric, electrostatic, and hydrophobicity parameters. Statistically significant 3D-QSAR models of the steroidal alkaloids inhibitors were designed by exploring the multiple conformations of each ligand using the genetic algorithm. An alignment technique scheme was generated from the docking results, and it yielded highly predictive 3D-QSAR models. The good correlation observed in all cases of 3D-QSAR supports the proposed method of alignment and selection of conformers.

The models were validated by the prediction of inhibitory activities of the test set compounds. In terms of external predictions, CoMSIA and CoMFA both performed great; however, their comparison showed that CoMSIA is better

than CoMFA for this data set. A comparison of the 3D-QSAR PLS coefficient contour maps with the structural and functional features of the binding sites also showed good correlation. It is evident from the contour plots of the both analyses that the hydrophobic effect plays main contribution to the BuChE inhibitory activity and its quite in agreement with the fact that the BuChE is having a wide active site gorge. Also, the bulky groups in the side chain at the R2 position generally cause the increase in activity, but at the same time the bulkier substituent at the position R3 resulted in decreasing the activity. This R3 position is covered by a yellow steric contour, and hence showing the bulkiness at this region is detrimental to the activity. The preference for the bulky group at position R2 as described in CoMFA seems to be correlated in CoMSIA with an increased hydrophobicity expected at the same region. As the first attempt to exploiting the BuChE inhibitors for the 3D-QSAR approach combined with all the detailed information obtained by 3D-QSAR models, we strongly believe that this study can help to design novel molecules to possess improved activity in near future.

The results, together with the good correlations between the actual and predicted inhibitory activities, demonstrate the power of the combined docking/QSAR approach to explore the probable binding conformations of compounds at the active sites of the protein target. Additionally, the present study also demonstrates that charges resulting from different calculation methods may influence the results of CoMFA as well as CoMSIA, although in our case this effect has not been significant. This is evident from the q^2 values calculated for different charge calculation methods (Supporting Information).

ACKNOWLEDGMENT

Financial support from the Higher Education Commission, Pakistan to R.U. under the Split Ph.D. program is highly acknowledged. The authors are grateful to the Pakistan Science Foundation (PSF) for the financial support to develop computer software facilities at the ICCBS.

Supporting Information Available: FlexX generated pose of the cocrystallized ligand superimposed with the crystal structure (Figure S1), influence of the different charges on predictive model (Table S1), and scheme for the overall procedure applied during this 3D-QSAR modeling (Figure S2). This material is available free of charge via the Internet at <http://pubs.acs.org>.

REFERENCES AND NOTES

- Butters, N.; Delis, D. C.; Lucas, J. A. Clinical assessment of memory disorders in amnesia and dementia. *Annu. Rev. Psychol.* **1995**, *46*, 493–523.
- Giacobini, E. Cholinesterases: new roles in brain function and in Alzheimer's disease. *Neurochem. Res.* **2003**, *28* (3–4), 515–22.
- Terry, A. V.; Buccafusco, J. J. The cholinergic hypothesis of age and Alzheimer's disease-related cognitive deficits: recent challenges and their implications for novel drug development. *J. Pharmacol. Exp. Ther.* **2003**, *306* (3), 821–7.
- Soreq, H.; Zaku, H. *Human Cholinesterases and Anticholinesterases*; Academic Press: San Diego, 1993.
- Massoulie, J.; Sussman, J.; Bon, S.; Silman, I. Structure and functions of acetylcholinesterase and butyrylcholinesterase. *Prog. Brain Res.* **1993**, *98*, 139–46.
- Cokugras, A. N. Butyrylcholinesterase: structure and physiological importance. *Turk. J. Biochem.* **2003**, *28* (2), 54–61.
- Meshorer, E.; Erb, C.; Gazit, R.; Pavlovsky, L.; Kaufer, D.; Friedman, A.; Glick, D.; Ben-Arie, N.; Soreq, H. Alternative splicing and neuritic mRNA translocation under long-term neuronal hypersensitivity. *Science* **2002**, *295* (5554), 508–12.
- Behra, M.; Cousin, X.; Bertrand, C.; Vonesch, J. L.; Biellmann, D.; Chatonnet, A.; Strahle, U. Acetylcholinesterase is required for neuronal and muscular development in the zebrafish embryo. *Nat. Neurosci.* **2002**, *5* (2), 111–8.
- Bazelyansky, M.; Robey, E.; Kirsch, J. F. Fractional diffusion-limited component of reactions catalyzed by acetylcholinesterase. *Biochemistry* **1986**, *25* (1), 125–30.
- Lockridge, O.; Masson, P. Pesticides and susceptible populations: people with butyrylcholinesterase genetic variants may be at risk. *Neurotoxicology* **2000**, *21* (1–2), 113–26.
- Massoulie, J.; Pezzementi, L.; Bon, S.; Krejci, E.; Vallette, F. M. Molecular and cellular biology of cholinesterases. *Prog. Neurobiol.* **1993**, *41* (1), 31–91.
- Xie, W.; Stribley, J. A.; Chatonnet, A.; Wilder, P. J.; Rizzino, A.; McComb, R. D.; Taylor, P.; Hinrichs, S. H.; Lockridge, O. Postnatal developmental delay and supersensitivity to organophosphate in gene-targeted mice lacking acetylcholinesterase. *J. Pharmacol. Exp. Ther.* **2000**, *293* (3), 896–902.
- Chatonnet, A.; Lockridge, O. Comparison of butyrylcholinesterase and acetylcholinesterase. *Biochem. J.* **1989**, *260* (3), 625–34.
- Mack, A.; Robitzki, A. The key role of butyrylcholinesterase during neurogenesis and neural disorders: an antisense-5'-butyrylcholinesterase-DNA study. *Prog. Neurobiol.* **2000**, *60* (6), 607–28.
- Greig, N. H.; Utsuki, T.; Yu, Q.; Zhu, X.; Holloway, H. W.; Perry, T.; Lee, B.; Ingram, D. K.; Lahiri, D. K. A new therapeutic target in Alzheimer's disease treatment: attention to butyrylcholinesterase. *Curr. Med. Res. Opin.* **2001**, *17* (3), 159–65.
- Giacobini, E. Metabolic relations between glia and neurons studied in single cells. In *Morphological and Biochemical Correlates of Neural Activity*; Hoeber, N. Y.; Synder, R. S., Eds.; Harper & Row: New York, 1964; pp 15–38.
- Graybiel, A. M.; Ragsdale, C. W., Jr. Pseudocholinesterase staining in the primary visual pathway of the macaque monkey. *Nature* **1982**, *299* (5882), 439–42.
- Guillozet, A. L.; Smiley, J. F.; Mash, D. C.; Mesulam, M. M. Butyrylcholinesterase in the life cycle of amyloid plaques. *Ann. Neurol.* **1997**, *42* (6), 909–18.
- Barber, K. L.; Mesulam, M. M.; Kraft, G.; Klein, W. L. Butyrylcholinesterase (BuChE) alters the aggregation state of A β amyloid. In *Society for Neuroscience's Abstract*; Washington, DC, 1996; Vol. 22, p 1172.
- Lehmann, D. J.; Johnston, C.; Smith, A. D. Synergy between the genes for butyrylcholinesterase K variant and apolipoprotein E4 in late-onset confirmed Alzheimer's disease. *Hum. Mol. Genet.* **1997**, *6* (11), 1933–6.
- Yu, Q.; Holloway, H. W.; Flippen-Anderson, J. L.; Hoffman, B.; Brossi, A.; Greig, N. H. Methyl analogues of the experimental Alzheimer drug phenserine: synthesis and structure/activity relationships for acetyl- and butyrylcholinesterase inhibitory action. *J. Med. Chem.* **2001**, *44* (24), 4062–71.
- Yu, Q.; Holloway, H. W.; Utsuki, T.; Brossi, A.; Greig, N. H. Synthesis of novel phenserine-based-selective inhibitors of butyrylcholinesterase for Alzheimer's disease. *J. Med. Chem.* **1999**, *42* (10), 1855–61.
- Giacobini, E. Cholinesterase inhibitors: from the Calabar bean to Alzheimer therapy. In *Cholinesterases and Cholinesterase Inhibitors*; Giacobini, E., Ed.; Martin Dunitz: London, 2000; pp 181–226.
- Giacobini, E.; Griffini, P. L. In The effect of MF-8622: a selective BuChE inhibitor. *Proceedings of the Society for Neuroscience*; Washington, DC, 1996; p 203.
- Greig, N. H.; De Micheli, E.; Holloway, H. W.; Yu, Q. S.; Utsuki, T.; Perry, T. A.; Brossi, A.; Ingram, D. K.; Deutsch, J.; Lahiri, D. K.; Soncrant, T. T. The experimental Alzheimer drug phenserine: pre-clinical pharmacokinetics and pharmacodynamics. *Acta. Neurol. Scand. Suppl.* **2000**, *176*, 74–84.
- Ikari, H.; Spangler, E. L.; Greig, N. H.; Pei, X. F.; Brossi, A.; Speer, D.; Patel, N.; Ingram, D. K. Maze learning in aged rats is enhanced by phenserine, a novel anticholinesterase. *NeuroReport* **1995**, *6* (3), 481–4.
- Greig, N. H.; Utsuki, T.; Ingram, D. K.; Wang, Y.; Pepeu, G.; Scali, C.; Yu, Q. S.; Mamczarz, J.; Holloway, H. W.; Giordano, T.; Chen, D.; Furukawa, K.; Sambamurti, K.; Brossi, A.; Lahiri, D. K. Selective butyrylcholinesterase inhibition elevates brain acetylcholine, augments learning and lowers Alzheimer beta-amyloid peptide in rodent. *Proc. Natl. Acad. Sci. U.S.A.* **2005**, *102* (47), 17213–8.
- Sussman, J. L.; Harel, M.; Frolow, F.; Oefner, C.; Goldman, A.; Tokier, L.; Silman, I. Atomic structure of acetylcholinesterase from *Torpedo californica*: a prototypic acetylcholine-binding protein. *Science* **1991**, *253* (5022), 872–9.

- (29) Harel, M.; Sussman, J. L.; Krejci, E.; Bon, S.; Chanal, P.; Massoulie, J.; Silman, I. Conversion of acetylcholinesterase to butyrylcholinesterase: modeling and mutagenesis. *Proc. Natl. Acad. Sci. U.S.A.* **1992**, *89* (22), 10827–31.
- (30) Bourne, Y.; Taylor, P.; Marchot, P. Acetylcholinesterase inhibition by fasciculins: crystal structure of the complex. *Cell* **1995**, *83* (3), 503–512.
- (31) Doorn, J. A.; Talley, T. T.; Thompson, C. M.; Richardson, R. J. Probing the active sites of butyrylcholinesterase and cholesterol esterase with isomalathion: conserved stereoselective inactivation of serine hydrolases structurally related to acetylcholinesterase. *Chem. Res. Toxicol.* **2001**, *14* (7), 807–13.
- (32) Nachon, F.; Nicolet, Y.; Masson, P. Butyrylcholinesterase: 3D structure, catalytic mechanisms. *Ann. Pharm. Fr.* **2005**, *63* (3), 194–206.
- (33) Nicolet, Y.; Lockridge, O.; Masson, P.; Fontecilla-Camps, J. C.; Nachon, F. Crystal structure of human butyrylcholinesterase and of its complexes with substrate and products. *J. Biol. Chem.* **2003**, *278* (42), 41141–7.
- (34) Tormos, J. R.; Wiley, K. L.; Seravalli, J.; Nachon, F.; Masson, P.; Nicolet, Y.; Quinn, D. M. The reactant state for substrate-activated turnover of acetylthiocholine by butyrylcholinesterase is a tetrahedral intermediate. *J. Am. Chem. Soc.* **2005**, *127* (42), 14538–9.
- (35) Nachon, F.; Asojo, O. A.; Borgstahl, G. E.; Masson, P.; Lockridge, O. Role of water in aging of human butyrylcholinesterase inhibited by echothiophate: the crystal structure suggests two alternative mechanisms of aging. *Biochemistry* **2005**, *44* (4), 1154–62.
- (36) Saxena, A.; Redman, A. M.; Jiang, X.; Lockridge, O.; Doctor, B. P. Differences in active site gorge dimensions of cholinesterases revealed by binding of inhibitors to human butyrylcholinesterase. *Biochemistry* **1997**, *36* (48), 14642–51.
- (37) Saxena, A.; Redman, A. M.; Jiang, X.; Lockridge, O.; Doctor, B. P. Differences in active-site gorge dimensions of cholinesterases revealed by binding of inhibitors to human butyrylcholinesterase. *Chem.-Biol. Interact.* **1999**, *119–120*, 61–9.
- (38) Radic, Z.; Pickering, N. A.; Vellom, D. C.; Camp, S.; Taylor, P. Three distinct domains in the cholinesterase molecule confer selectivity for acetyl- and butyrylcholinesterase inhibitors. *Biochemistry* **1993**, *32* (45), 12074–84.
- (39) Perry, E. K.; Tomlinson, B. E.; Blessed, G.; Bergmann, K.; Gibson, P. H.; Perry, R. H. Correlation of cholinergic abnormalities with senile plaques and mental test scores in senile dementia. *Br. Med. J.* **1978**, *2* (6150), 1457–1459.
- (40) Cho, S. J.; Garsia, M. L.; Bier, J.; Tropsha, A. Structure-based alignment and comparative molecular field analysis of acetylcholinesterase inhibitors. *J. Med. Chem.* **1996**, *39* (26), 5064–71.
- (41) Tame, J. R. Scoring functions: a view from the bench. *J. Comput.-Aided Mol. Des.* **1999**, *13* (2), 99–108.
- (42) Donini, O. A.; Kollman, P. A. Calculation and prediction of binding free energies for the matrix metalloproteinases. *J. Med. Chem.* **2000**, *43* (22), 4180–8.
- (43) Cramer Iii, R. D.; Patterson, D. E.; Bunce, J. D. Comparative molecular field analysis (CoMFA). I. Effect of shape on binding of steroids to carrier proteins. *J. Am. Chem. Soc.* **1988**, *110* (18), 5959–5967.
- (44) Klebe, G.; Abraham, U.; Mietzner, T. Molecular similarity indices in a comparative analysis (CoMSIA) of drug molecules to correlate and predict their biological activity. *J. Med. Chem.* **1994**, *37* (24), 4130–46.
- (45) Prathipati, P.; Pandey, G.; Saxena, A. K. CoMFA and docking studies on glycogen phosphorylase inhibitors as antidiabetic agents. *J. Chem. Inf. Model.* **2005**, *45* (1), 136–45.
- (46) Debnath, A. K. Three-dimensional quantitative structure-activity relationship study on cyclic urea derivatives as HIV-1 protease inhibitors: application of comparative molecular field analysis. *J. Med. Chem.* **1999**, *42* (2), 249–59.
- (47) Klebe, G. Comparative molecular similarity indices analysis: CoMSIA. *Perspect. Drug Discovery Des.* **1998**, *12*, 87–104.
- (48) Bohm, M.; St rzebecher, J.; Klebe, G. Three-dimensional quantitative structure-activity relationship analyses using comparative molecular field analysis and comparative molecular similarity indices analysis to elucidate selectivity differences of inhibitors binding to trypsin, thrombin, and factor Xa. *J. Med. Chem.* **1999**, *42* (3), 458–77.
- (49) Atta ur, R.; Zaheer ul, H.; Feroz, F.; Khalid, A.; Nawaz, S. A.; Khan, M. R.; Choudhary, M. I. New Cholinesterase-Inhibiting Steroidal Alkaloids from *Sarcococca saligna*. *Helv. Chim. Acta* **2004**, *87*, 439.
- (50) Atta ur, R.; Feroz, F.; Naeem, I.; Zaheer ul, H.; Nawaz, S. A.; Khan, N.; Khan, M. R.; Choudhary, M. I. New pregnane-type steroidal alkaloids from *Sarcococca saligna* and their cholinesterase inhibitory activity. *Steroids* **2004**, *69* (11–12), 735–41.
- (51) Atta ur, R.; Choudhary, M. I.; Khan, M. R.; Anjum, S.; Farooq, A.; Iqbal, M. Z. New steroidal alkaloids from *Sarcococca saligna*. *J. Nat. Prod.* **2000**, *63* (10), 1364–8.
- (52) Atta ur, R.; Zaheer ul, H.; Khalid, A.; Anjum, S.; Khan, M. R.; Choudhary, M. I. Pregnane-type Steroidal Alkaloids of *Sarcococca saligna*: A New Class of Cholinesterases Inhibitors. *Helv. Chim. Acta* **2002**, *85*, 678–688.
- (53) Kalauni, S. K.; Choudhary, M. I.; Shaheen, F.; Manandhar, M. D.; Atta ur, R.; Gewali, M. B.; Khalid, A. Steroidal alkaloids from the leaves of *Sarcococca coriacea* of Nepalese origin. *J. Nat. Prod.* **2001**, *64* (6), 842–4.
- (54) Khalid, A.; Zaheer ul, H.; Anjum, S.; Khan, M. R.; Atta ur, R.; Choudhary, M. I. Kinetics and structure-activity relationship studies on pregnane-type steroidal alkaloids that inhibit cholinesterases. *Bioorg. Med. Chem.* **2004**, *12* (9), 1995–2003.
- (55) Zaheer ul, H.; Wellenzohn, B.; Tonmuphean, S.; Khalid, A.; Choudhary, M. I.; Rode, B. M. 3D-QSAR studies on natural acetylcholinesterase inhibitors of *Sarcococca saligna* by comparative molecular field analysis (CoMFA). *Bioorg. Med. Chem. Lett.* **2003**, *13* (24), 4375–80.
- (56) Zaheer ul, H.; Wellenzohn, B.; Liedl, K. R.; Rode, B. M. Molecular docking studies of natural cholinesterase-inhibiting steroidal alkaloids from *Sarcococca saligna*. *J. Med. Chem.* **2003**, *46* (23), 5087–90.
- (57) Khalid, A.; Zaheer ul, H.; Ghayur, M. N.; Feroz, F.; Atta ur, R.; Gilani, A. H.; Choudhary, M. I. Cholinesterase inhibitory and spasmolytic potential of steroidal alkaloids. *J. Steroid Biochem. Mol. Biol.* **2004**, *92* (5), 477–84.
- (58) Dominguez, C.; Boelens, R.; Bonvin, A. M. HADDOCK: a protein-protein docking approach based on biochemical or biophysical information. *J. Am. Chem. Soc.* **2003**, *125* (7), 1731–7.
- (59) Jain, A. N. Surflex: fully automatic flexible molecular docking using a molecular similarity-based search engine. *J. Med. Chem.* **2003**, *46* (4), 499–511.
- (60) Johnson, M. A.; Hoog, C.; Pinto, B. M. A novel modeling protocol for protein receptors guided by bound-ligand conformation. *Biochemistry* **2003**, *42* (7), 1842–53.
- (61) Sabnis, Y. A.; Desai, P. V.; Rosenthal, P. J.; Avery, M. A. Probing the structure of falcipain-3, a cysteine protease from *Plasmodium falciparum*: comparative protein modeling and docking studies. *Protein Sci.* **2003**, *12* (3), 501–9.
- (62) Todorov, N. P.; Mancera, R. L.; Monthoux, P. H. A new quantum stochastic tunnelling optimisation method for protein-ligand docking. *Chem. Phys. Lett.* **2003**, *369*, 257–263.
- (63) Vicker, N.; Ho, Y.; Robinson, J.; Woo, L. L.; Purohit, A.; Reed, M. J.; Potter, B. V. Docking studies of sulphamate inhibitors of estrone sulphatase in human carbonic anhydrase II. *Bioorg. Med. Chem. Lett.* **2003**, *13* (5), 863–5.
- (64) Wang, L.; Merz, A. J.; Collins, K. M.; Wickner, W. Hierarchy of protein assembly at the vertex ring domain for yeast vacuole docking and fusion. *J. Cell Biol.* **2003**, *160* (3), 365–74.
- (65) Wu, X.; Milne, J. L.; Borgnia, M. J.; Rostapshov, A. V.; Subramaniam, S.; Brooks, B. R. A core-weighted fitting method for docking atomic structures into low-resolution maps: application to cryo-electron microscopy. *J. Struct. Biol.* **2003**, *141* (1), 63–76.
- (66) Zhou, Z.; Fisher, D.; Spidel, J.; Greenfield, J.; Patson, B.; Fazal, A.; Wigal, C.; Moe, O. A.; Madura, J. D. Kinetic and docking studies of the interaction of quinones with the quinone reductase active site. *Biochemistry* **2003**, *42* (7), 1985–94.
- (67) Wei, H. Y.; Tsai, K. C.; Lin, T. H. Modeling Ligand-Receptor Interaction for Some MHC Class II HLA-DR4 Peptide Mimetic Inhibitors Using Several Molecular Docking and 3D QSAR Techniques. *J. Chem. Inf. Model.* **2005**, *45* (5), 1343–1351.
- (68) Pan, X.; Tan, N.; Zeng, G.; Han, H.; Huang, H. 3D-QSAR and docking studies of aldehyde inhibitors of human cathepsin K. *Bioorg. Med. Chem.* **2006**, *14* (8), 2771–2778.
- (69) Medina-Franco, J. L.; Rodríguez-Morales, S.; Juárez-Gordiano, C.; Hernández-Campos, A.; Castillo, R. Docking-based CoMFA and CoMSIA studies of non-nucleoside reverse transcriptase inhibitors of the pyridinone derivative type. *J. Comput.-Aided Mol. Des.* **2004**, *18* (5), 345–360.
- (70) Hu, X.; Stebbins, C. E. Molecular docking and 3D-QSAR studies of Yersinia protein tyrosine phosphatase YopH inhibitors. *Bioorg. Med. Chem.* **2005**, *13* (4), 1101–9.
- (71) Buolamwini, J. K.; Assefa, H. CoMFA and CoMSIA 3D QSAR and docking studies on conformationally-restrained cinnamoyl HIV-1 integrase inhibitors: exploration of a binding mode at the active site. *J. Med. Chem.* **2002**, *45* (4), 841–852.
- (72) Yuan, H.; Kozikowski, A. P.; Petukhov, P. A. CoMFA study of piperidine analogues of cocaine at the dopamine transporter: exploring the binding mode of the 3 α -substituent of the piperidine ring using pharmacophore-based flexible alignment. *J. Med. Chem.* **2004**, *47* (25), 6137–43.
- (73) Yuan, H.; Petukhov, P. A. Improved 3D-QSAR CoMFA of the dopamine transporter blockers with multiple conformations using the genetic algorithm. *Bioorg. Med. Chem. Lett.* **2006**, *16* (24), 6267–72.
- (74) Holland, J. H. *Adaptation in natural and artificial systems*; University of Michigan Press: Ann Arbor, MI, 1975.
- (75) Forrest, S. Genetic algorithms: principles of natural selection applied to computation. *Science* **1993**, *261* (5123), 872.

- (76) Goldberg, D. E. *Genetic Algorithm in Search, Optimization and Machine Learning*; Addison-Wesley Professional: Reading, MA, 1989; p 170–174.
- (77) Fogel, L. J.; Owens, A. J.; Walsh, M. J. *Artificial Intelligence Through Simulated Evolution*; Wiley: New York, 1966.
- (78) Atta ur, R.; Feroz, F.; Zaheer ul, H.; Nawaz, S. A.; Khan, M. R.; Choudhary, M. I. New steroidal alkaloids from *Sarcococca saligna*. *Nat. Prod. Res.* **2003**, *17* (4), 235–41.
- (79) Sybyl, version 7.2; Tripos International: St. Louis, MO, 2006.
- (80) Clark, M.; Cramer, R. D.; Van Opdenbosch, N. Validation of the general purpose tripos 5. 2 force field. *J. Comput. Chem.* **1989**, *10* (8), 982–1012.
- (81) Rarey, M.; Kramer, B.; Lengauer, T.; Klebe, G. A fast flexible docking method using an incremental construction algorithm. *J. Mol. Biol.* **1996**, *261* (3), 470–489.
- (82) Lemmen, C.; Lengauer, T.; Klebe, G. FLEXS: a method for fast flexible ligand superposition. *J. Med. Chem.* **1998**, *41* (23), 4502–4520.
- (83) Viswanadhan, V. N.; Ghose, A. K.; Revankar, G. R.; Robins, R. K. Atomic physicochemical parameters for three dimensional structure directed quantitative structure-activity relationships. 4. Additional parameters for hydrophobic and dispersive interactions and their application for an automated superposition of certain naturally occurring nucleoside antibiotics. *J. Chem. Inf. Comput. Sci.* **1989**, *29* (3), 163–172.
- (84) Geladi, P.; Kowalski, B. R. Partial Least Squares: A Tutorial. *Anal. Chim. Acta* **1986**, *185*, 1–17 .

CI8000056